A Novel Alkali-Activated Cement from Mineral Admixture, Superabsorbent Polymers, and Alkali-Doped Carboxylate Glass

Min Qu[a], Fazhou Wang[a,*], Peng Liu[b], Donald E Macphee[c], Chuanlin Hu[a,*], Lu Yang[a]

[a] *State Key Laboratory of Silicate Materials for Architectures, Wuhan University of Technology, Wuhan 430070, PR China*

[b] *School of chemistry, chemical engineering and life science, Wuhan University of Technology, Wuhan 430070, PR China*

[c] *Department of Chemistry, University of Aberdeen, Meston Building, Meston Walk, AB24 3UE Aberdeen, Scotland, United Kingdom*

*Corresponding author: Prof. Fazhou Wang, State Key Laboratory of Silicate Materials for Architectures, Wuhan University of Technology, Email: fzhwang@whut.edu.cn; Chuanlin Hu, State Key Laboratory of Silicate Materials for Architectures, Wuhan University of Technology, Email: chuanlin@whut.edu.cn.

Abstract

In this paper, we introduce a novel approach for the targeted delivery of concentrated alkali required for activation of aluminosilicate-based cements, which avoids exposure to caustic solutions on site. The solid alkali, encapsulated within a water-soluble glass (alkali-doped carboxylate glass) is dry blended with mineral admixtures (ground granulated blast slag and fly ash) and water saturated superabsorbent polymers (SAP, being the only source of mix water in this study). The solubility of alkali-doped carboxylate glasses (ACG) was characterized. The hydration of ground granulated blast slag (GGBS) and fly ash (FA) with different curing times were monitored by SEM, XRD, FT-IR and solid-state MAS NMR, which showed the co-existence of calcium aluminum silicate hydrate (C-A-S-H) gel and sodium aluminosilicate hydrate (N-A-S-H) gel in the hydration products. The mechanical properties of AAC were tested, and the compressive strength of AAC (using ACG as alkali activator, water saturated SAP as water source) reached over 40 MPa after curing for 28 days.

Keywords: alkali-activated cement; alkali-doped carboxylate glass; superabsorbent polymer; SEM; solid-state NMR.

1. Introduction

The reaction of an alkali source with an alumina- and silica-containing solid precursor to form a solid material (i.e., alkali-activated materials) was found comparable to hardened Portland cement and first patented by Jasper in 1908 [1]. Alkali-activated materials (AAMs), also known as alkali-activated cement (AAC), can be designed to have superior properties compared with binders prepared from OPC, with regard to acids and sulfate resistance [2], strength [3], heat resistance [4], low greenhouse gas emissions and environmental impact [5], etc. Nevertheless, several practical issues such as the handling of caustic materials on site, supply chains for raw materials and inadequate testing protocols limit the industrial acceptance of AAC [6, 7].

Advanced techniques for internal curing that can sustain the needed chemical environment (e.g., moisture, basicity) are straightforward solutions to improving the properties of AAC [8]. SAP have been used as a porous lightweight aggregate and internal curing agent in cements as they are non-toxic, have a high capacity for water absorption and allow a high level of water retention [9, 10]; water is released from the SAP during cement hydration due to osmotic pressure and differential humidity effects [11, 12]. Additionally, SAP can be saturated with water in advance and then transported at ease, hence alleviating the accessibility of water for blending solid procurers in special areas, e.g., deserts or other areas without access to potable water sources.

Aside from the hydration reaction, the activation of the solid aluminosilicate precursor by alkali is another critical performance-defining parameter for AAC. Conventional AAMs are formed by reaction between a concentrated aqueous solution of alkali activator [13, 14] and solid aluminosilicate precursor (such as fly ash, ground granulated blast slag which are already well-known and wide applications in AAMs [15]). These are known as two- part AAMs. However, the impracticalities related to handling large amounts of viscous, corrosive, and operationally onerous alkali activator solutions, limit the usage of AAC compared with OPC [6]. Subsequently, one-part (or "just add water") AAMs were developed which contained a solid source of alkali [16-18], e.g. Na_2SiO_3, mixed with a solid aluminosilicate precursorhe compressive strengths are

usually lower in comparison with similar composition two-part AAMs [19]. Besides, operational challenges were still taxing because the solid alkali can easily absorb water and CO_2 in the air and lose effectiveness. We explore here the effectiveness of 'slow' release glasses, as a means of controlled release and delivery of alkali *in situ*. Such glasses are produced at low temperature (<350 ℃) from the organic salt of alkali metals and previous studies on matrices for controlled release of bioactive materials[20], have depended on their water solubility. In the present application, encapsulation of alkali in a slow-release glass is expected to protect the alkali from CO_2 and control the rate of its release. For greater alkalization effect, such glasses can also be used to encapsulate fine particles of solid alkali (e.g. NaOH). The alkali-doped glass can be dry mixed with the solid aluminosilicate precursor so that the alkali is dispersed prior to water addition. The carboxylate glass readily dissolved in water, provides high alkali concentrations locally to act as an alkali activator for GGBS and FA. Besides, by altering the alkali release rate of ACG, we could effectively control the reaction degree of the system to satisfy the specific mechanical property.

Hence in this work, we developed a ternary alkali-activated cement system based on GGBS and FA with ACG as the alkali activator and water saturated SAP as the water source.

2. Materials and methods

2.1. Materials

GGBS was obtained from the Masteel group. Fly ash (FA) was obtained from the Huaneng Yangluo power station. The oxide compositions of the GGBS and the FA were characterized by X-ray fluorescence spectrometry (XRF) and shown in Table 1. The particle size distribution of GGBS and FA was obtained from laser diffraction (Mastersizer 2000) and was shown in S1, which indicated the mean particle size and median particle diameter of 14.64 and 11.25μm, respectively, for slag, and 18.62 and 11.27μm, respectively, for FA.

Table 1. Composition of GGBS and FA from X-ray fluorescence analysis.

Oxide (wt%)	SiO_2	Al_2O_3	Fe_2O_3	CaO	K_2O	MgO	Na_2O	SO_3	LOI
GGBS	33.31	15.30	0.39	39.58	0.41	7.89	0.60	2.17	-1.20
Fly ash	55.35	30.94	3.24	2.39	1.01	0.57	0.47	0.37	3.85

The superabsorbent polymers (SAP, 50-200 μm, d_{50} = 107μm) were purchased from the Shanghai Chen Qi Chemical Technology Co., Ltd. Sodium hydroxide, sodium acetate, lithium acetate, sodium octanoate and other chemicals were purchased from Shenshi Chem. All chemicals were of analytical grade. Doubly distilled water was used in all experiments.

2.2. **Preparation of** alkali-doped carboxylate glass **(ACG)**

The use of slow-release media to deliver alkalis in cement systems has not been widely reported previously but a significant contribution to understanding how to prepare and characterize alkali-bearing, low melting point, mixed carboxylate glasses has been made by Hansen et al [21]. The methodologies described have been adopted in this work for the preparation and characterisation of ACG as follows:

NaOH pellets were dried in an oven over night at 100 °C prior to use and ground in a mortar to fine powder. Certain mixtures of alkali metal carboxylate were mixed in a Pyrex beaker, and heated on a hot-plate (320 °C) until all crystal water is evaporated (no more bubbles form). Pre-heated NaOH powder was slowly added under stirring (the heating should not be too long to avoid charring the mixture) and the melt was finally quenched on an ice-cooled metal plate. The composition of the ACG used in this study is listed in Table 2.

Table 2. Formulations of alkali-doped carboxylate glasses (ACG).

Formulation of Components	Molecular Ratio
$Na(CH_3COO)\cdot 3H_2O$	1
$Li(CH_3COO)\cdot 2H_2O$	1.3
$CH_3(CH_2)_6COONa$	0.4
$Ca(OH)_2$	0.2
NaOH	1.5

2.3. Preparation of alkali-activated cement pastes and cubes

Alkali-activated cement pastes were prepared by mixing the binders (GGBS and FA), the alkali activator (ACG or NaOH solutions), and the water source (using water saturated SAP or using water directly) and stirring the mixture at 160 rpm for 5 min to form homogeneous pastes, which were then cast in cubic stainless-steel moulds (40 mm × 40 mm × 40 mm). The filled moulds were vibrated for 60 s to liberate the trapped air bubbles, covered with a plastic film to prevent the evaporation of water, and the pastes were then cured at room temperature for 1, 7 and 28 days to produce hardened cubes. The formulations of these three groups of AAC cubes are shown in Table 3.

Table 3. Formulation of alkali-activated cement pastes.

Sample Group	Binders	Alkali Activator*	Water Source	liquid-to-solid ratio
1	GGBS & FA*	NaOH solutions	water	0.40
2		ACG	water	

3		ACG	water saturated SAP

* The mass ratio of GGBS and FA was 4:1 in all sample groups. The amount of alkali used in all sample groups was, in the equivalent of Na_2O, 8% by mass of the solid binders.

2.4. Characterizations

2.4.1 Solubility and shelf-life test of alkali-doped carboxylate glass (ACG)

The solubility of ACG was measured by conductivity measurements together with pH measurement [21]. The glass-to-water weight ratio in the solubility test was constantly 1:10. Prior to solubility measurement, the glasses were ground and sieved in a nitrogen-filled atmosphere bag to defined sizes, 1-2 mm. Agitation was achieved with a magnetic stirring during all measurements and the measuring chamber was kept at constant temperature (25 °C) and with the surface constantly flushed with N_2.

The shelf-life of ACG was measured by the following method [21]: ACG was sieved, such that particles were restricted to a diameter of 1-2 mm, placed in weighting boats in desiccators and kept at either 32% relative humidity (RH) (saturated $CaCl_2$) or 81 % RH (saturated $(NH_4)_2SO_4$). Results shown are averages of 2 or 3 measurements.

2.4.2 Mechanical properties of alkali-activated cement pastes and cubes

The compressive strength of AAC cubes were tested with an automated hydraulic testing machine at a constant loading rate of 300 N/s. Four cement blocks were tested for each formulation/curing combination and the average and standard deviation were reported.

2.4.3 X-ray diffraction (XRD), Scanning electron microscopy (SEM) and solid-state magic angle spinning nuclear magnetic resonance (MAS NMR) spectra test

To evaluate the properties of AAC cubes, a fragment was chipped from the hardened cement cube and immersed in isopropanol for 24 h, then immersed in fresh isopropanol for another 6 days to fully displace the free water to thus terminate the

hydration reaction. The fragment was then dried in a vacuum oven (DZF-6090) at 40 °C for 24 h and ground in an agate mortar. The resulting powders were passed through a sieve (75 μm aperture) and analyzed by SEM, XRD, IR and solid-state MAS NMR.

X-ray diffraction (XRD, Empyrean) patterns were recorded at a scan rate of 5°/min over 2θ = 5-70° using Cu Kα radiation at 40 kV and 50 mA. Fourier transform infrared spectra (FT-IR) were obtained on a Nicolet Nexus 870 (Thermo Fisher) instrument in the range 4000 to 400 cm^{-1} with a resolution of 0.019 cm^{-1} [22].

Scanning electron microscopy (SEM) was carried out using a QUANTA FEG 450 instrument at an accelerating voltage of 15 keV with a spot size of 3.5 nm and a working distance of 10 mm. Samples for SEM analysis were made conductive by coating with Pt and then analyzed immediately in high vacuum mode using secondary electron imaging [23].

The solid-state magic angle spinning nuclear magnetic resonance (MAS NMR) spectra of ^{29}Si and ^{27}Al were recorded on a Bruker Advance III 400 MHz NMR spectrometer (Billerica, MA) with a field strength of 9.8 T. The chemical shift of ^{29}Si was referenced to tetrakis(trimethylsilyl)silane (TTMS) at −9.8 ppm, and the chemical shift of ^{27}Al was referenced to the saturated solution of $Al(NO_3)_3$ in H_2O at 0.0 ppm [24].

3. Results and discussion

3.1. Solubility and shelf-life of alkali-doped carboxylate glasses (ACG)

The development of alkalinity in the cement pore water of these cements is expected due to the dissolution of the carboxylate glass. This effect is monitored by the changing conductivity of the solution with time (see Fig 1) which also shows the increase in pH associated with the release of alkali from the glass.

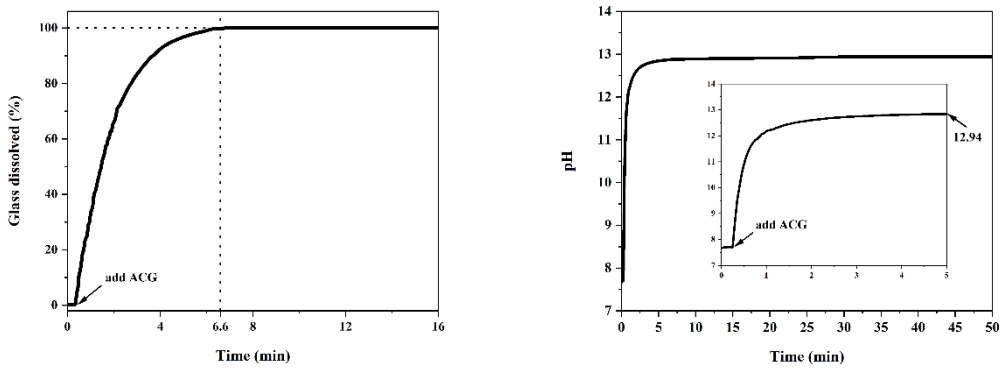

(a) (b)

Fig. 1. (a) Glasses dissolution curves (conductivity as % of total). (b) pH changes curves of glasses dissolution.

Glasses (size=2 mm) were dissolved at a 10.0% glass-to-water mass ratio.

Under these test conditions, after 6.6 minutes, ACG was completely dissolved, and the pH reached 12.94.

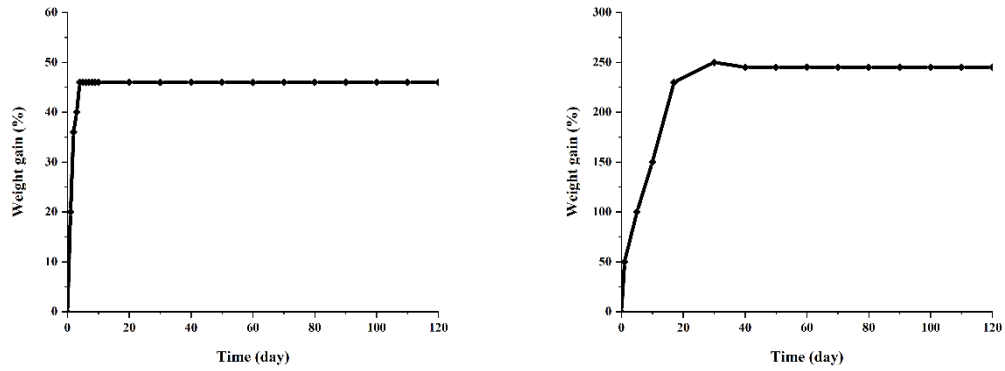

(a) (b)

Fig. 2. Weight gain (%) of ACG. Glass pieces (1-2 mm) were stored in a desiccator of (a) 32% or (b) 81% relative humidity.

Fig. 2 shows the water absorption by ACG (glass pieces, with diameter of 1-2 mm) at different relative humidities (RH). At 32% RH, the ACG had gained 46% weight after 4 days, then steady state appeared to have been reached. At 81% RH, ACG had gained over 230% weight after 17 days after which the weight remained constant. These

data indicate that the surface becomes water saturated at a level which is RH dependent; it seems that the ACG hadn't fully dissolved in the water absorbed.

3.2. Compressive strength

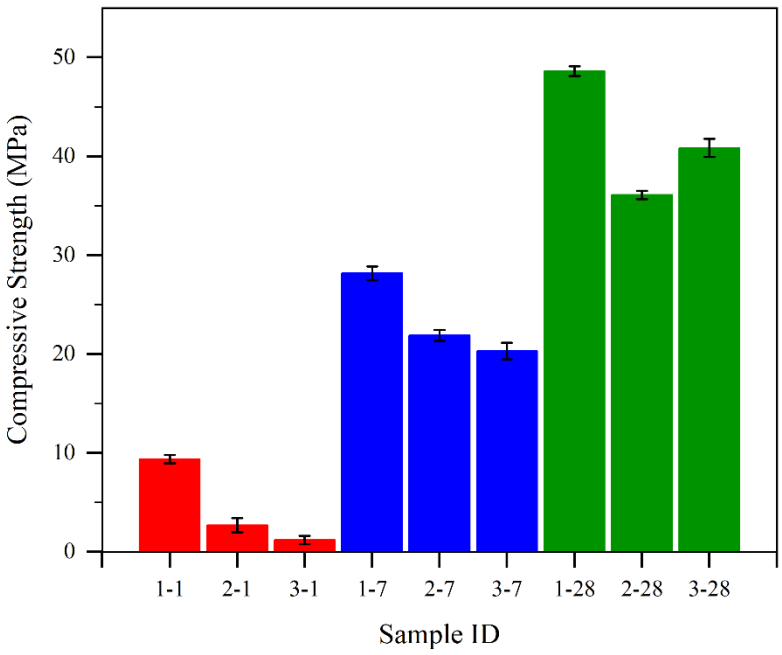

Fig. 3. The compressive strength results of AAC cubes.

(* The identifier of "x-y", x means the sample group, y means the curing times.)

Fig. 3 showed the compressive strength development of cement cubes cured up to 28 days. When cured for 1 day, the strength of 1-1 reached about 10 MPa, while the strength of 2-1 and 3-1 was very low. With increasing curing time, all cement cubes obtained development of compressive strength. It was worth remarking that the compressive strength of 3-7 was lower than 2-7 but 3-28 was higher than 2-28, which could be attributed to the performance of internal curing effect by SAP.

3.3. Scanning electron microscopy (SEM) images

Fig. 4 shows the SEM images of precursor (GGBS and FA) and AAC with

different curing times. When curing for 1 day, in 1-1, the FA beads lost their spherical surface and the GGBS particles lost their edges and corners, while the morphology of FA and GGBS in 2-1 and 3-1 only changed slightly and represented a low degree of reaction for the FA and GGBS.

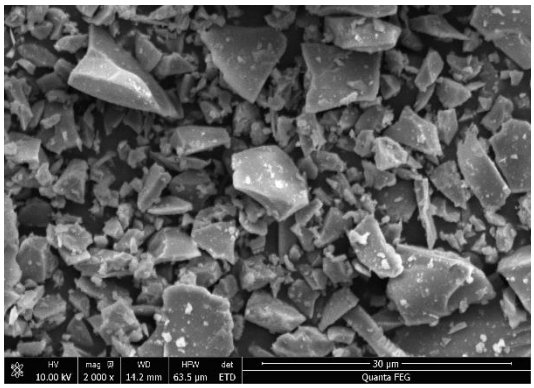

(a)

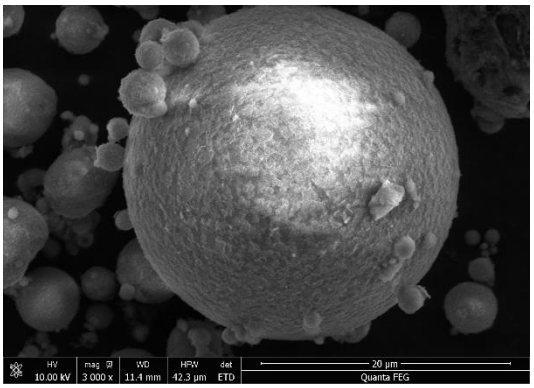

(b)

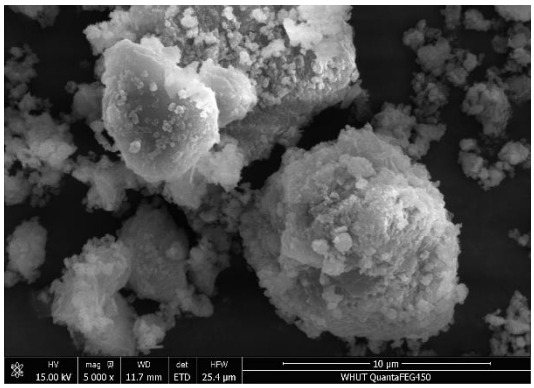

(c)

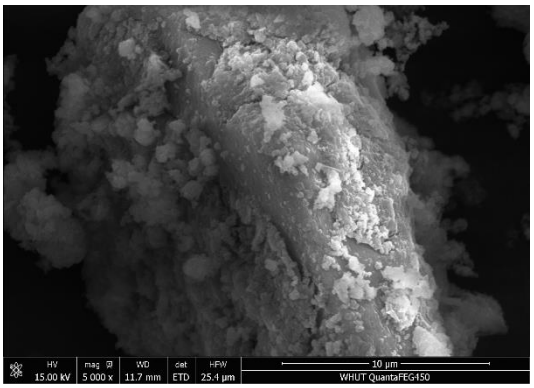

(d)

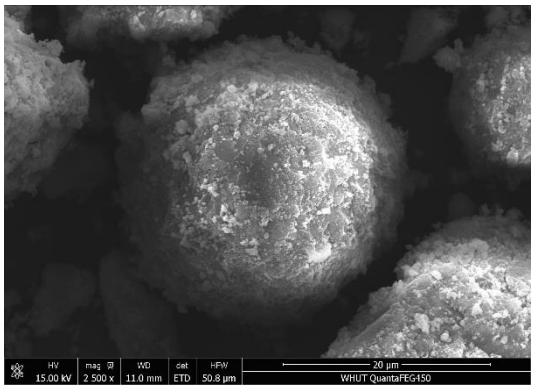

(e)

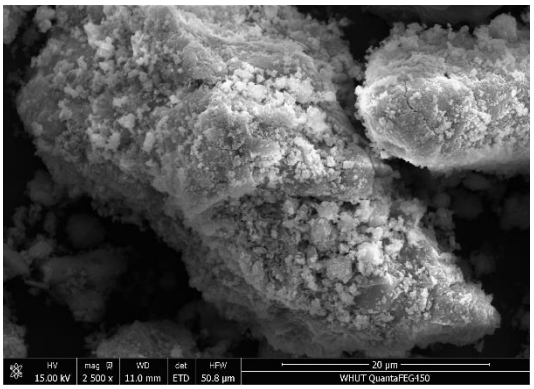

(f)

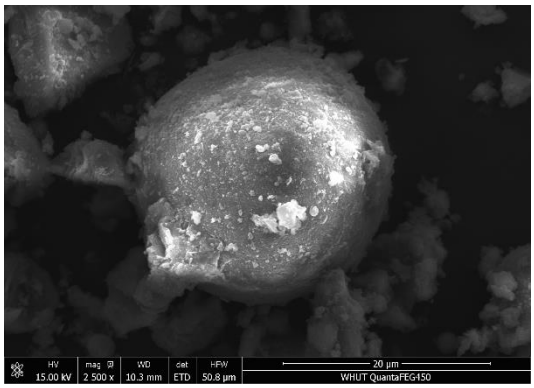
HV
15.00 kV
mag
2 500 x
WD
10.3 mm
det
ETD
HFW
50.8 µm
20 µm
WHUT QuantaFEG450

(g)

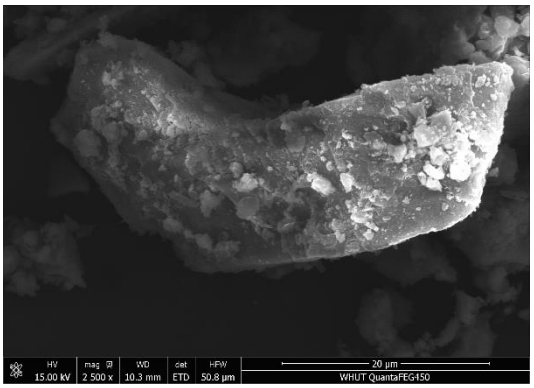
HV
15.00 kV
mag
2 500 x
WD
10.3 mm
det
ETD
HFW
50.8 µm
20 µm
WHUT QuantaFEG450

(h)

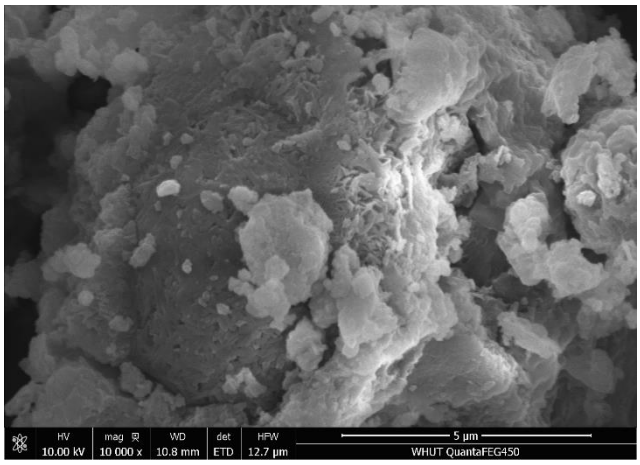
HV
10.00 kV
mag
10 000 x
WD
10.8 mm
det
ETD
HFW
12.7 µm
5 µm
WHUT QuantaFEG450

(i)

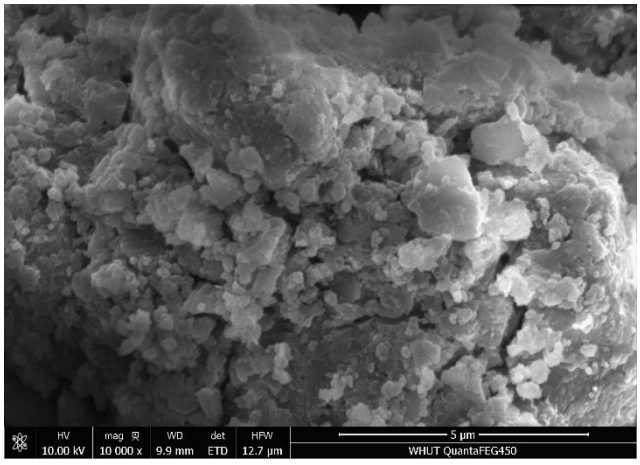
HV
10.00 kV
mag
10 000 x
WD
9.9 mm
det
ETD
HFW
12.7 µm
5 µm
WHUT QuantaFEG450

(j)

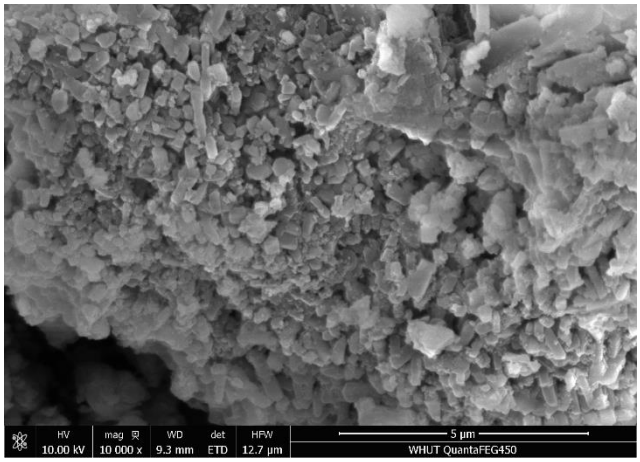

(k)

Fig. 4. SEM images of (a) unreacted GGBS, (b) unreacted FA, (c) GGBS particles in sample 1-1, (d) FA particles in sample1-1, (e) GGBS particles in sample 2-1, (f) FA particles in sample 2-1, (g) GGBS particles in sample 3-1, (h) FA particles in sample3-1, (i) sample 1-28, (j) sample 2-28, (k) sample 3-28.

Group 1 (corresponding to sample 1-1) used NaOH solutions (as alkali activator) and water (as water source) directly. Group 2 (corresponding to sample 2-1) used ACG as alkali activator. Alkali needed to be dissolved from ACG into the mix water system to activate GGBS and FA, which gave a reason for the low reaction degree of group 2 in the early curing time.

In group 3 (corresponding to sample 3-1), the alkali activator was ACG and the water source was water saturated SAP. The water should be released from SAP first and then ACG could be dissolved to release alkali into the system to activate GGBS and FA, which caused the low reaction degree of group 3 in the early curing time. This accounts for the observations from the compressive strength data.

After curing for 28 days, the SEM images of all groups (sample 1-28, 2-28 and 3-28) demonstrated a high reaction degree, with hydration products coating the aluminosilicate substrates in all cases, with some of the observed dense hydrates resembling the N-A-S-H gel reported by Provis [25].

When water and alkali are used directly, the alkali activation reaction is fast and products form quickly on substrate surfaces. Product coating of substrate particles in

close contact might easily reduce the accessibility of substrate surface to sustained exposure to alkali by closing inter-particle channels. Alkali strength in reacting regions is reduced by the consumption of alkali which means that, without an accessible supply of suitably concentrated alkali, reactivity in closed pores may be limited and stop after porosity is sealed by reaction products. When using ACG (as alkali activator; Group 2), reaction in closed pores can continue provided there is retained water to dissolve the ACG, this being further enhanced by the availability of SAP in group 3 samples. The slower kinetics governing the release of alkali (Figure 1) may also partially account for the slower development in strength.

3.4. X-ray diffraction (XRD)

In Fig. 5, the shift of 2θ peaks from lower value in GGBS and FA to higher value in the AAC was characteristic of the development of the amorphous phase [26]. The XRD powder pattern has features consistent with N-A-S-H [27] and C-A-S-H gels, with weak Bragg reflections recorded between 27.5° and 35°. Hydrotalcite ($Mg_6Al_2(CO_3)(OH)_{16}\cdot 4H_2O$, PDF# 00-04a-1428) was observed in all samples. This is consistent with the findings of other studies on the alkali-activation of GGBS containing akermanite ($Ca_2MgSi_2O_7$) and gehlenite ($Ca_2Al_2SiO_7$) [28]. Moreover, a zeolite product with a gismondine type [29] structure was also identified in the samples. The reflections of quartz (SiO_2, PDF# 00-046-1045) and mullite ($Al_6Si_2O_{13}$, PDF# 00-015-0776) were also detected, likely to be the crystalline phases of residual FA particles that did not participate in the alkali activation reaction [30].

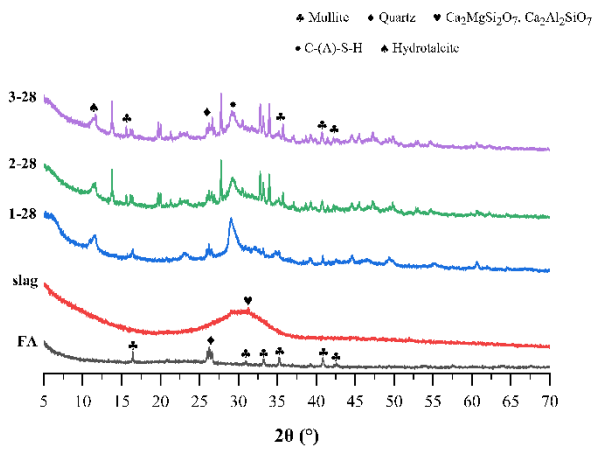

Fig. 5. XRD patterns of GGBS, FA and AAC curing for 28 days.

3.5. Fourier-transform infrared (FT-IR) spectroscopy

Fig. 6 shows the FTIR spectra of GGBS, FA and AAC curing for 28 days, and Table 5 provided the assignment of the individual peaks. The peak at around 1000 cm^{-1} could be associated with the asymmetric vibrations generated by T-O-T bonds (where T is Si or Al) [31] in the C-A-S-H gel. In all groups of AAC, the location of peak assigned to ν_3 (Si-O) in FA is narrowed and shifts to lower wavenumbers in different groups. These shifts indicate that the original aluminosilicate structures were significantly depolymerized to form the N-A-S-H gel [32]. With the replacement of Si^{4+} by Al^{3+}, the peak shape of T-O-T became sharper, the peak shifting to lower wavenumbers because the Al-O bond is longer and weaker than the Si-O bond [33].

The spectra of all samples show a new peak at 1640-1660 cm^{-1} after the alkali activation. This peak can be attributed to the bending vibrations of O-H and indicates the presence of structural water in the reaction products [34]. The peak at 1400 cm^{-1} was assigned to carbonation of samples about the formation of calcium carbonate [35]. The small peak at 420 cm^{-1} results from the bending vibration of the O-Si-O bond [35] and can be associated with quartz and unreacted precursor [33, 34].

Table 5. IR absorption peaks of GGBS, FA, and AAC.

Peak No.	Wavenumber (cm^{-1})	Group Name
1	3500	Stretching Vibration of H-O-H
2	1640-1660	Bending vibrations of O-H
3	1400	Asymmetric stretching of C-O-C bonds
4	1000-1100	Asymmetric vibrations of T-O-T bonds (T = Si or Al)

5	420	Bending vibration of O-Si-O bonds

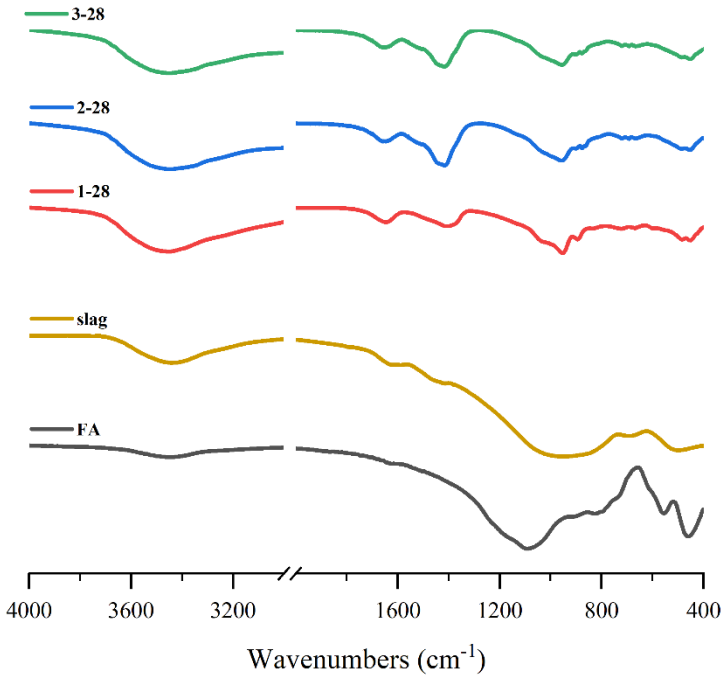

Fig. 6. FT-IR spectra of unreacted GGBS and FA, and AAC curing for 28 days.

3.6. Solid state magic angle spinning nuclear magnetic resonance (solid-state MAS NMR) spectroscopy

3.6.1. ^{27}Al solid-state MAS NMR

Fig. 7 shows NMR spectra of ^{27}Al solid-state MAS for GGBS, FA and AAC with different curing times. It could be seen that 4-coordinated, 5-coordinated and 6-coordinated Al could be clearly distinguished from each other.

The spectrum of the unreacted GGBS showed a broad and asymmetric resonance and could be deconvoluted into two peaks, one centered around 61 ppm, which was assigned to 4-coordinated Al units, and other centered around 37 ppm, which was assigned to 5-coordinated Al units. These peaks were attributed to the major glassy phases in GGBS, consistent with the amorphous hump detected in the GGBS by XRD

(shown in Fig. 5). FA contained two broad peaks and were assigned to 6-coordinated (2 ppm) and 4-coordinated (51 ppm) Al units, where the 6-coordinated units corresponded to Al in mullite and mullite-like glassy phases [36], and the 4-coordinated units were Al substituted in silicate glasses [37].

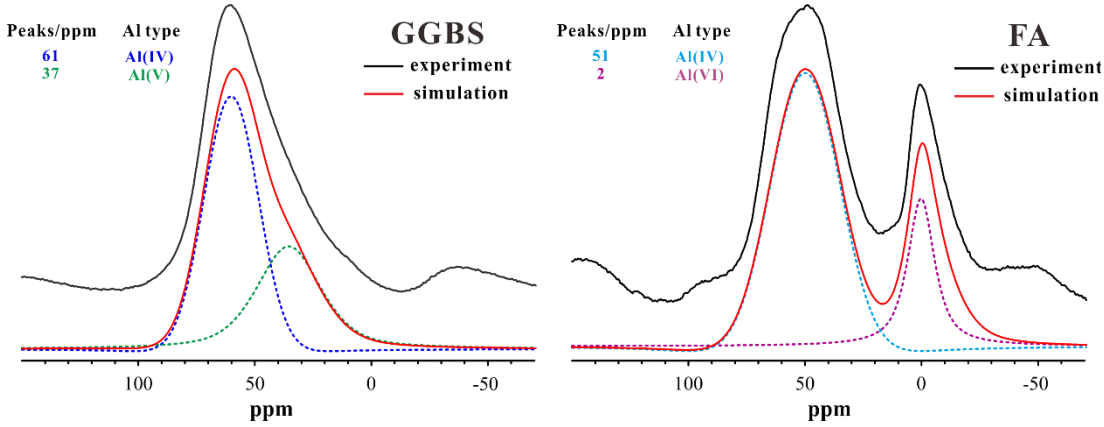

(a)

(b)

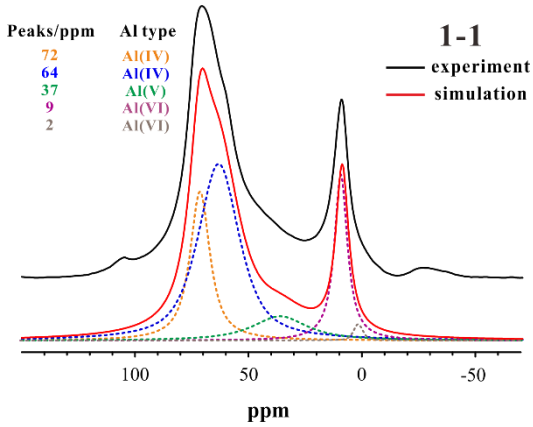

(c)

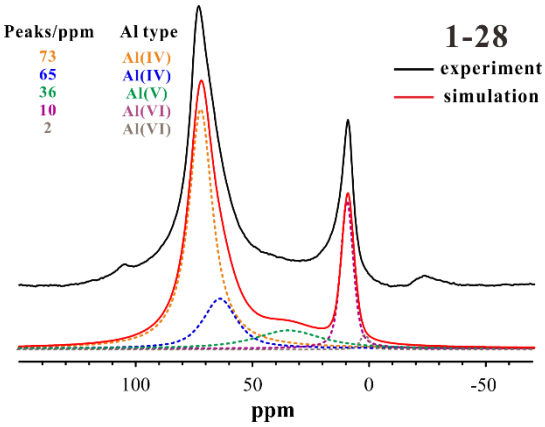

(d)

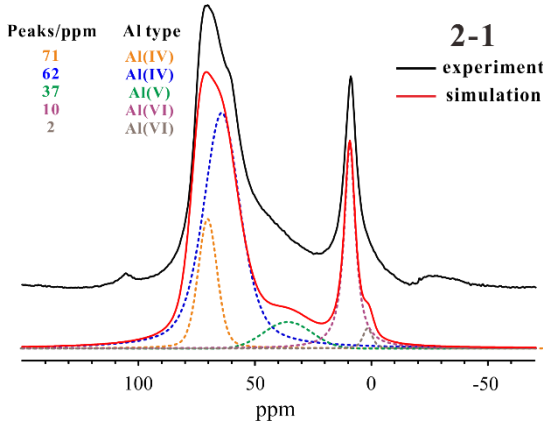

(e)

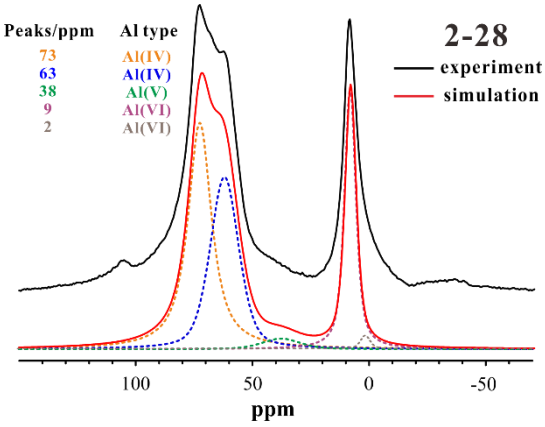

(f)

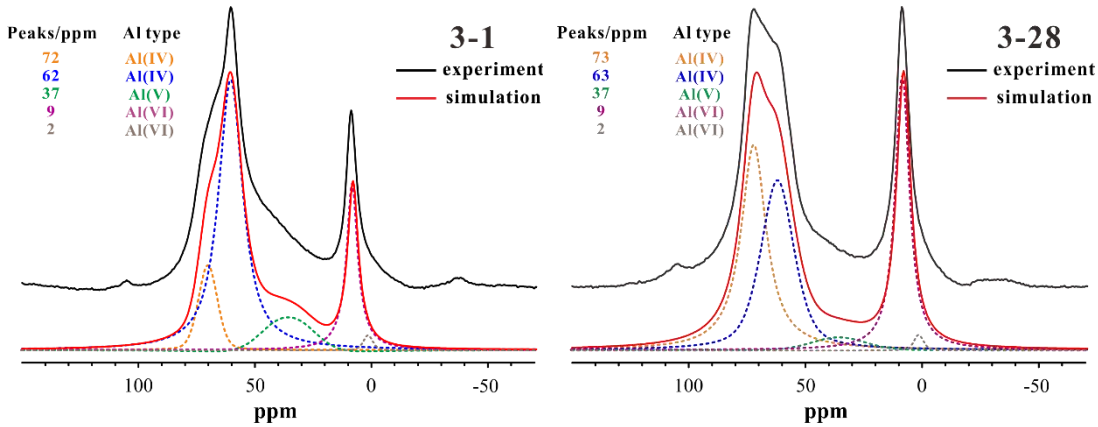

(g) (h)

Fig. 7. Deconvolution results for the ^{27}Al solid-state MAS NMR spectra of unreacted GGBS and FA, and AAC with different curing times. The simulation is the sum of the deconvoluted peaks.

(Identified with different colored dotted curves for each Si types.)

Table 6. Deconvolution results from ^{27}Al solid-state MAS NMR spectra of unreacted GGBS, FA and AAC with different curing times. Molar fractions of ^{27}Al in different chemical environment were listed.

Sample ID	Molar fractions of ^{27}Al in different chemical environment	
	^{27}Al in reaction products	^{27}Al in unreacted precursors
GGBS	/	100.0 %
FA	/	100.0 %
1-1	53.4 %	46.6 %
1-28	85.2 %	14.8 %
2-1	40.3 %	59.7 %
2-28	66.7 %	33.3%
3-1	37.1 %	62.9 %
3-28	65.0 %	35.0 %

After alkali activation, as shown in Fig. 7, all the samples exhibited five peaks, assigned as follows: 72 ± 1 ppm, assigned to 4-coordinated units and attributed to the Al incorporated in bridging tetrahedral bonded to Q^2(1Al) sites [38]; 63 ± 2 ppm and 37

± 1 ppm, assigned to 4-coordinated and 5-coordianted Al, respectively, and attributed to the Al in glassy phases of unreacted GGBS [39]; 9±1 ppm and 2 ppm, assigned to 6-coordinated Al units, and attributed to the Al in hydrotalcite [40] and in unreacted FA, respectively.

Table 6 summarises the changes in peak areas associated with hydration products and anhydrous starting materials over the range of AAC curing times, showing hydration rate information for each system, i.e. for conventional hydration, 85.2% of Al in anhydrous material is incorporated into hydration product in 28 days. For ACG/water and ACG/SAP activation, this reduces to 66.7% and 65% respectively.

3.6.2. ^{29}Si solid-state MAS NMR

The assignment of NMR components was based on reported values obtained from aluminosilicate [40, 41]. According to published data, the peaks were assigned as follows: from -66 to -73 ppm, Q^0 units; from -73 to -78 ppm, Q^1 units; from -83 to -88 ppm, Q^2 units; from -90 to -100 ppm, Q^3 units; from -100 to -115 ppm, Q^4 units. Because the substitution of Si by Al shifts the signal by 3 or 5 ppm towards the more positive values, the peak appearing at -80 to -84 ppm can be ascribed to Q^2(1Al). Fig. 8 shows that the GGBS only contained one peak at -73 ppm, which can be assigned to Q^1. In contrast, FA contained two peaks at -106 ppm and -90 ppm, which can be assigned to Q^4 and Q^3, respectively.

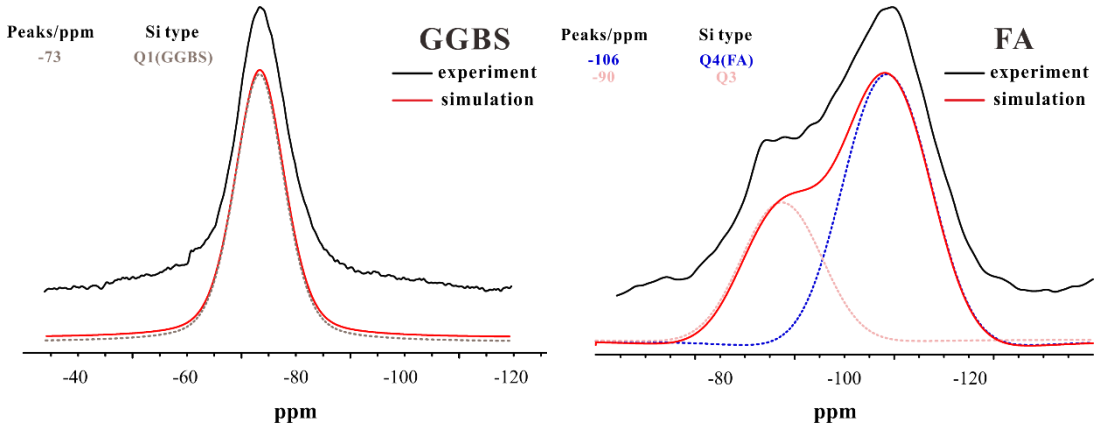

(a) (b)

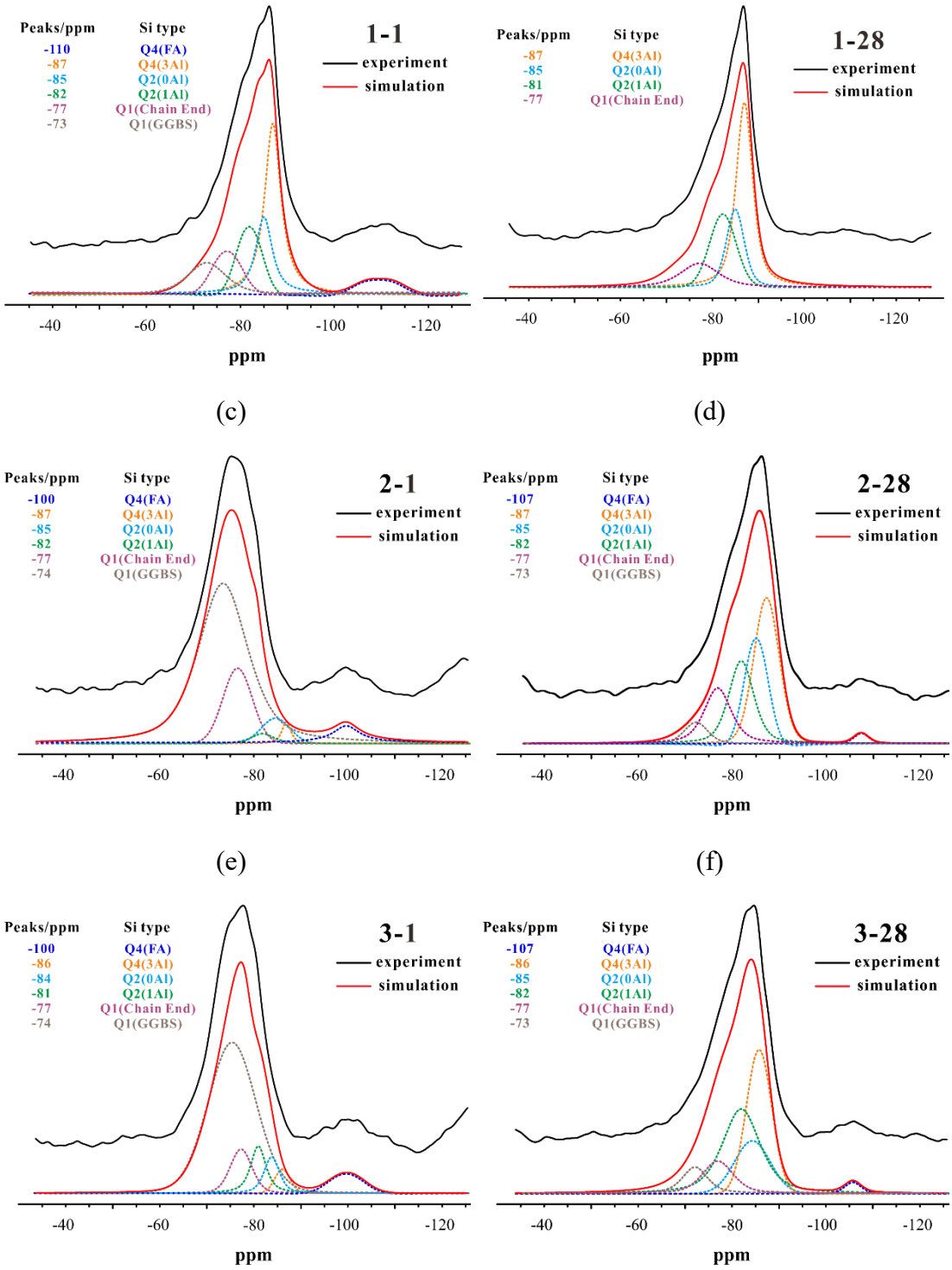

Fig. 8. Deconvolution results for ^{29}Si solid-state MAS NMR spectra of unreacted GGBS and FA, and AAC with different curing times. The simulation is the sum of the deconvoluted peaks.

(Identified with different colored dotted curves for each Si types)

Table 7. Deconvolution results from ^{29}Si solid-state MAS NMR spectra of unreacted GGBS, FA, and AAC with different curing times. Molar fractions of ^{29}Si in different chemical environment were listed.

Sample ID	Molar fractions of ^{29}Si in different chemical environment	
	^{29}Si in reaction products	^{29}Si in unreacted precursors
GGBS	/	100.0 %
FA	/	100.0 %
1-1	72.7 %	27.3 %
1-28	99.9 %	0.1 %
2-1	34.1 %	65.9 %
2-28	92.5 %	7.5 %
3-1	26.0 %	74.0 %
3-28	90.0 %	10.0 %

Figure 8 and Table 7 shows that after curing for 1 day, the relative intensity of the Q^1 peaks (at -73±1 ppm) from unreacted GGBS and the Q^4 peaks (at -105±5) from unreacted FA both decreased, hence indicated the occurrence of the alkali activation reaction. The decreases were much more pronounced for Sample 1-1 than for 2-1 and 3-1, illustrated that the reaction was much milder with activation by ACG and/or SAP. Upon extended curing, the relative intensity of Q^1(Chain End), Q^2(1Al), and Q^2(0Al) increased obviously, and the relative intensity of Q^1(GGBS) diminished, which indicated the chemical reactions intensified with time; the difference in the degree of reaction became smaller between Sample 1-28, 2-28, and 3-28.

It can be seen from Fig. 8 that new ^{29}Si solid-state MAS NMR peaks appear, additional to those in the spectra of unreacted GGBS and FA. Specifically, the peaks at -82±1 ppm and -85±1 ppm, corresponding to Q^2(1Al) and Q^2(0Al), thus confirming hydration and indicating the formation of an Al-substituted C-S-H type (C-A-S-H) gel

with a tobermorite type structure.

The peak at -87±1 ppm, which existed in the ^{29}Si solid-state MAS NMR spectra of all samples, can be assigned to $Q^4(3Al)$ and is attributed to the formation of N-A-S-H gel. The relative intensity of $Q^4(3Al)$ is very small in Sample 2-1 and 3-1, because without extensive curing, only a limited amount of FA was activated by alkali.

4. Conclusions

ACG has demonstrated its potential as an alkali activation vehicle for AAC systems. In the present study, it has exhibited comparable compressive strength development to that of AAC activated conventionally with aqueous NaOH. In addition, the incorporation of SAP benefits the compressive strength development, which can be attributed to the internal curing effect of SAP in the AAC system.

The main hydration products of GGBS and FA activation are not affected by the ACG approach and the studied systems included tobermorite-like C-A-S-H gel and three-dimensional cross-linked N-A-S-H gel as expected. The rate of hydration appears to be correlated with the availability of the alkali to the aqueous solution during hydration. Unlike with the significant excesses of alkalinity available instantly during conventional alkali activation, the glassy ACG releases it alkalinity slowly to avoid rapid local hydration and the closing of porosity between particles due to hydration products. This explains the slower rate of conversion of anhydrous materials to hydration products and correspondingly slower strength development but the rate of this process is also affected by the solubility of the ACG glass, a factor which can be modified in future products. Nevertheless, the present study showed a continuation of the hydration process in the ACG and ACG/SAP systems, attributable to the reserves of alkali and stored water.

Hence, a new ternary alkali-activated cement was successfully designed by using GGBS and FA as solid precursors, water saturated SAP as the water supplier and internal curing agent, and ACG as the alkali activator, respectively. This ternary alkali-activated cement can be potentially used for construction in remote under-developed

areas where construction conditions are challenging and shortage of raw materials exists. Besides, the mechanical properties of this novel AAC could be further enhanced by optimize the composition and proportion of raw materials, and the main emphasis of the research in future could focus on the formula design of ACG to control the alkali release at the desired rate.

5. Acknowledgments

We gratefully acknowledge the financial support of China National Key R&D Program (Grant No. 2018YFE0106300) and National Nature Science Foundation of China (No: 51925205).

We gratefully acknowledge the financial support of “111” project (No. B18038).

We gratefully acknowledge the Dr. Helle Rüsz Hansen for her contribution to the development of the slow release glasses used in this paper.

6. Reference

[1] Jasper Whiting. United States Patent No 544706, 20.08.1895.

[2] T. Bakharev, Resistance of geopolymer materials to acid attack, Cem. Concr. Res. 35 (2005) 658-670.

[3] A.M.M. Bakri, H. Kamarudin, M. Binhussain, Comparison of geopolymer fly ash and ordinary portland cement to the strength of concrete, Adv. Sci. Lett. 19 (2013) 3592-3595.

[4] P.K. Sarker, S. McBeath, Fire endurance of steel reinforced fly ash geopolymer concrete elements, Constr. Build. Mater. 90 (2015) 91-98.

[5] S. Espuelas, A.M. Echeverria, S Marcelino, Technical and environmental characterization of hydraulic and alkaline binders, J. Cleaner Prod.196 (2018) 1306-1313.

[6] P. Duxson, J.L. Provis, Designing precursors for geopolymer cements, J. Am. Ceram. Soc. 91 (2008) 3864-3869.

[7] J.S.J. van Deventer, J.L. Provis, P. Duxson, Technical and commercial progress in the

adoption of geopolymer cement, Miner. Eng. 29 (2012) 89-104.

[8] O.M. Jensen, P.F. Hansen, Water-entrained cement-based materials - I. Principles and theoretical background, Cem. Concr. Res. 31 (2001) 647-654.

[9] J. Justs, M. Wyrzykowski, D. Bajare, Internal curing by superabsorbent polymers in ultra-high performance concrete, Cem. Concr. Res. 76 (2015) 82-90.

[10] D. Snoeck, O.M. Jensen, N. De Belie, The influence of superabsorbent polymers on the autogenous shrinkage properties of cement pastes with supplementary cementitious materials, Cem. Concr. Res. 74 (2015) 59-67.

[11] F.Z. Wang, J Yang, Study on mechanism of desorption behavior of saturated superabsorbent polymers in concrete, ACI Materials Journal. 112 (2015) 460-470.

[12] F.Z. Wang, J Yang, S.G Hu, Influence of superabsorbent polymers on the surrounding cement paste, Cem. Concr. Res. 81 (2016) 116-121.

[13] P. Duxson, A. Fernández-Jiménez, J.L. Provis, Geopolymer technology: the current state of the art, J. Mater. Sci. 42 (2007) 2917-2933.

[14] J.L. Provis, Geopolymers and other alkali activated materials: why, how, and what? Mater. Struct. 47 (2014) 11-25.

[15] G Yıldırım, A Kul, E Özçelikci, Development of Alkali-Activated Binders from Recycled Mixed Masonry-originated Waste, J. Build. Eng. 33 (2021) 101690.

[16] A. Palomo, A. Fernández-Jiménez, C. López-Hombrados, Railway sleepers made of alkali activated fly ash concrete, Rev. Ing. Constr. 22 (2007) 75-80.

[17] A. Hajimohammadi, J.S.J. van Deventer, Characterization of one-part geopolymer binders made from fly ash, Waste Biom. Valor. 8 (2017) 225-233

[18] B. Nematollahi, J. Sanjayan, F.U.A. Shaikh, Comparative deflection hardening behavior of short fiber reinforced geopolymer composites, Constr. Build. Mater. 70 (2014) 54-64.

[19] B. Nematollahi, J. Sanjayan, F.U.A. Shaikh, Synthesis of heat and ambient cured one-part geopolymer mixes with different grades of sodium silicate, Ceram. Int. 41 (2015) 5696-5704.

[20] J.A. Blair, A.J. Mordue, Use of metal carboxylate glasses in the controlled release of bioactive molecules: Culex quinquefasciatues oviposition pheromone, J. Contr. Rel. 31 (1994) 145-149.

[21] H.R. Hansen, The alkali activation of aluminosilicate materials: mechanisms and practical

implementation, Internal Report, University of Aberdeen (2011).

[22] M.S. Kim, Y. Jun, C. Lee, Use of CaO as an activator for producing a price-competitive non-cement structural binder using ground granulated blast furnace slag, Cem. Concr. Res. 54 (2013) 208-214.

[23] R.J. Thomas, B.S. Gebregziabiher, Micromechanical properties of alkali-activated slag cement binders, Cem. Concr. Compos. 90 (2018) 241-256.

[24] B. Walkley, J.L. Provis, Solid-state nuclear magnetic resonance spectroscopy of cements, Mater Today Adv. 1 (2019) 100007.

[25] S.A. Bernal, J.L. Provis, B Walkley, Gel nanostructure in alkali-activated binders based on slag and fly ash, and effects of accelerated carbonation, Cem. Concr. Res. 53 (2013) 127-144.

[26] D. Khale, R. Chaudhary, Mechanism of geopolymerization and factors influencing its development: a review, J. Mater. Sci. 42 (2007) 729-746.

[27] M.T. Carrasco, J.G. Palomo, F. Puertas, Sodium silicate solutions from dissolution of glass wastes, Statistical analysis, Mater. Constr. 64 (2014) 314.

[28]H.M. Ben, B. Lothenbach, Influence of slag chemistry on the hydration of alkali-activated blast-furnace slag-Part I: Effect of MgO, Cem. Concr. Res. 41 (2011) 955-963.

[29] S.A. Bernal, J.L. Provis, D.G. Brice, Accelerated carbonation testing of alkali-activated binders significantly underestimate the real service life: the role of the pore solution, Cem. Concr. Res. 42 (10) (2012) 1317-1326.

[30] I Ismail, S.A. Bernal, J.L. Provis, Modification of phase evolution in alkali-activated blast furnace slag by the incorporation of fly ash. Cem. Concr. Compos. 45 (2014) 125-135.

[31] B. Walkley, R.S. Nicolas, M.A. Sani, Phase evolution of Na_2O-Al_2O_3-SiO_2-H_2O gels in synthetic aluminosilicate binders, Dalton Trans. 45 (2016) 5521-5535.

[32] W.K.W. Lee, J.S.J. van Deventer, Use of infrared spectroscopy to study geopolymerization of heterogeneous amorphous aluminosificates, Langmuir 19 (2003) 8726-8734.

[33] S.L.A. Valcke, P. Pipilikaki, H.R. Fischer, FT-IR and ^{29}Si-NMR for evaluating aluminium-silicate precursors for geopolymers, Mater. Struct. 48 (2015) 557-569.

[34] M. Krol, J. Minkiewicz, W. Mozgawa, IR spectroscopy studies of zeolites in geopolymeric materials derived from kaolinite, J. Mol. Struct. 1126 (2016) 200-206.

[35] S A. Bernal, J L. Provis, Gel nanostructure in alkali-activated binders based on slag and

fly ash, and effects of accelerated carbonation, Cem. Concr. Res. 53(2013) 127-144.

[36] L.H. Merwin, A. Sebald, H. Rager, ^{29}Si and ^{27}Al MAS NMR spectroscopy of mullite, Phys. Chem. Miner. 18 (1991) 47-52.

[37] A. Palomo, S. Alonso, A. Fernández-Jiménez, Alkaline activation of fly ashes: NMR study of the reaction products, J. Am. Ceram. Soc. 87 (2004) 1141-1145.

[38] S.D. Wang, K.L. Scrivener, ^{29}Si and ^{27}Al NMR study of alkali-activated slag, Cem. Concr. Res. 33 (2003) 769-774.

[39] P.J. Schilling, L.G. Butler, A. Roy, ^{29}Si and^{27}Al MAS-NMR of NaOH activated blast furnace slag, J. Am. Ceram. Soc. 77 (1994) 2363-2368.

[40] I.G. Richardson, A.R. Brough, G.W. Groves, Characterisation of hardened alkali-activated blast furnace slag pastes and the nature of the calcium silicate hydrate (CSH). Cem. Concr. Res. 5 (1994) 813-829.

[41] I.G. Richardson, A.R. Brough, R. Brydson, Location of aluminium in substituted calcium silicate hydrate (CSH) gels as determined by ^{29}Si and ^{27}Al NMR and EELS. J. Am Ceram. Soc. 76(1993) 2285-2288.